Ionic Covalent Organic Framework as a Dual Functional Sensor for Temperature and Humidity

Gobinda Das, Fayrouz Abou Ibrahim, Zahraa Abou Khalil, Philippe Bazin, Falguni Chandra, Rasha G Abdulhalim, Thirumurugan Prakasam, Akshaya Kumar Das, Sudhir Kumar Sharma, Sabu Varghese, et al.

Ionic Covalent Organic Framework as a Dual Functional Sensor for Temperature and Humidity

Gobinda Das, [a] # Fayrouz Abou Ibrahim, [a] # Zahraa Abou Khalil, [b] Philippe Bazin, [b] Falguni Chandra, [c] Rasha G. AbdulHalim, [a] Thirumurugan Prakasam, [a] Akshaya Kumar Das, [a] Sudhir Kumar Sharma, [d] Sabu Varghese, [e] Serdal Kirmizialtin, [a] Ramesh Jagannathan, [d] Na'il Saleh, [c] Farah Benyettou,[a] Mohamad El Roz, [b] Matthew Addicoat, [g] Mark A. Olson,[h] D.S. Shankar Rao,[i] S. Krishna Prasad,[j] and Ali Trabolsi *[a, i]

[a] Chemistry Program, New York University Abu Dhabi (NYUAD), Saadiyat Island, United Arab Emirates.
E-mail: ali.trabolsi@nyu.edu

[b] Laboratoire Catalyse et Spectrochimie, CNRS, Ensicaen, Université de Caen 6, Boulevard Maréchal Juin 14050, Caen, France.

[c] Chemistry Department, College of Science, United Arab Emirates University, P.O. Box 15551, Al-Ain, United Arab Emirates.

[d] Engineering Division, New York University Abu Dhabi (NYUAD), United Arab Emirates.

[e] CTP, New York University Abu Dhabi, 129188 Abu Dhabi, United Arab Emirates .

[f] National Water and Energy center, United Arab Emirates University, P.O. Box 15551, Al Ain, United Arab Emirates

[g] School of Science and Technology, Nottingham Trent University, Clifton Lane, NG11 8NS Nottingham, U.K.

[h] Department of Physical and Environmental Sciences, Texas A&M University Corpus Christi, 6300 Ocean Dr., Corpus Christi, TX 78412 USA.

[i] NYUAD Water Research Center, New York University Abu Dhabi (NYUAD), Saadiyat Island, United Arab Emirates

[j] Centre for Nano and Soft Matter Sciences, 560013 Bangalore, India.

Supporting information for this article is given via a link at the end of the document.

# These authors contributed equally to this work

Abstract: Visual sensing of humidity and temperature by solids plays an important role in our everyday life and in industrial processes. Due to their hydrophobic nature, most COF sensors often exhibit poor optical response when exposed to moisture. To overcome this challenge, we set out to improve the optical response to moisture by incorporating H-bonding ionic functionalities into the COF network. A highly sensitive COF, consisting of guanidinium and diformylpyridine linkers (TG-DFP), capable of detecting changes in temperature and moisture content was fabricated. The hydrophilic nature of the framework enables enhanced water uptake, allowing the trapped water molecules to form a large number of hydrogen bonds. Despite the presence of non-emissive building blocks, the H-bonds restrict internal bond rotation within the COF, leading to reversible fluorescence and solid-state optical hydrochromism in response to relative humidity and temperature.

Introduction

The development of optical-based sensors to detect changes in "environmental" properties" such as temperature[1] and humidity[1e, 2] has attracted considerable interest because of their significant impact on both the human health/life[3] and industrial sector.[1f, 2a-c, 3d, 4] Relative humidity (RH) - the concentration of water vapor in the air - has received considerable attention in scientific research due to its importance in all industries, from predictive maintenance in construction and infrastructure,[5] humidity control in the textile industry,[4d, 6] humidity monitoring in agriculture,[7] and production and storage in the food industry,[8] to all aspects of water sensing in healthcare facilities,[9] pharmaceutical processing,[10] and drug storage.[11] To date, known moisture-sensitive organic materials have been limited to small organic molecules,[2b, 4i, 12] [13], supramolecular nanostructures[2d, 12b, 13a, 14] polymeric materials,[14d, 15] and metal organic frameworks (MOFs).[16] However, the lack of long-range order in smaller molecular units and polymeric materials would compromise either stability, reusability, or precise tunability. Metal organic frameworks (MOFs), on the other hand, do not suffer from the above problems because they are crystalline, modifiable networks.[14f, 16b-f, 17] However, their high density and often poor hydrolytic stability would hinder their commercial applications.[18] To address these challenges, covalent organic frameworks (COFs) have been developed in recent years to serve as multivariate sensors for various types of external stimuli via the florescence response.[19] COF sensors are low mass density materials, offer excellent thermal and chemical stability,[19c, 20] coupled with tunable porosity and selectivity for guest molecules, making them outstanding candidates for sensing.[21] Real-time on-site humidity visualization with high sensitivity and accuracy using fluorescent or optical signals via a color-changing mechanism in a thermochromic luminophore is therefore a desired powerful tool in this regard.[2a, 22] Although some progress has been made in COF materials as fluorescent water sensors,[23] research in the area of COF water sensors is still in its infancy,[21b, 24]. Moreover, most COF optical sensors are often fabricated for specific applications and focus on a single function.[19c, 20a, 20b, 20d, 21a, 21b, 23b] In addition to RH detection, temperature detection using fluorescence is in high demand as a non-invasive method.[25] Consequently, the use temperature sensors is equally necessary.[26] The development of temperature sensors which can operate over a wide temperature range and especially under extreme conditions, such as high or low temperatures, pose a great challenge because organic-based luminescent materials may encounter diminished stability or suppressed sensor sensitivity at low temperatures, which can adversely affect their overall performance and reliability.[4g, 27] To date, fluorescent 2D and 3D COFs have been developed to exhibit luminescence at either room temperature or higher temperatures.[4g, 21b, 26-27] Luminescent materials capable of

emitting light at low temperatures hold significant potential for various applications, such as temperature sensors for products that need to be cooled or frozen. The concept of a dual-function COF sensor that is sensitive to both temperature and humidity is new and has not been widely explored.[24c] Therefore, there is an urgent need to develop an advanced, readable sensor that can monitor both temperature and RH in a single intelligent system. For real-world applications, solid-state fluorescent probes are a much more practical alternative. However, most COFs exhibit poor luminescence under wet conditions. This is either due to their inherent hydrophobic nature leading to poor polar interactions with atmospheric moisture or competition with non-radiative pathways causing effects such as aggregation-caused quenching (ACQ).[28] To improve the water tolerance of COF fluorophores, we recently reported luminescent ionic covalent organic frameworks (iCOFs) equipped with highly polar or charged hydrogen-bonded guanidinium functional groups.[21a] These hydrogen bonds block the pathway of non-radiative energy decay by restricting intramolecular bond rotation (RIR),[29] which enhances fluorescence.[24c, 28] In our previous work, we hypothesized that the introduction of H-bonded ionic electron-deficient moieties into the iCOF networks could improve the polarity of the iCOF surface, and thus the luminescence properties at intermediate humidity, by preventing the molecular motion of the iCOF network.[21a]

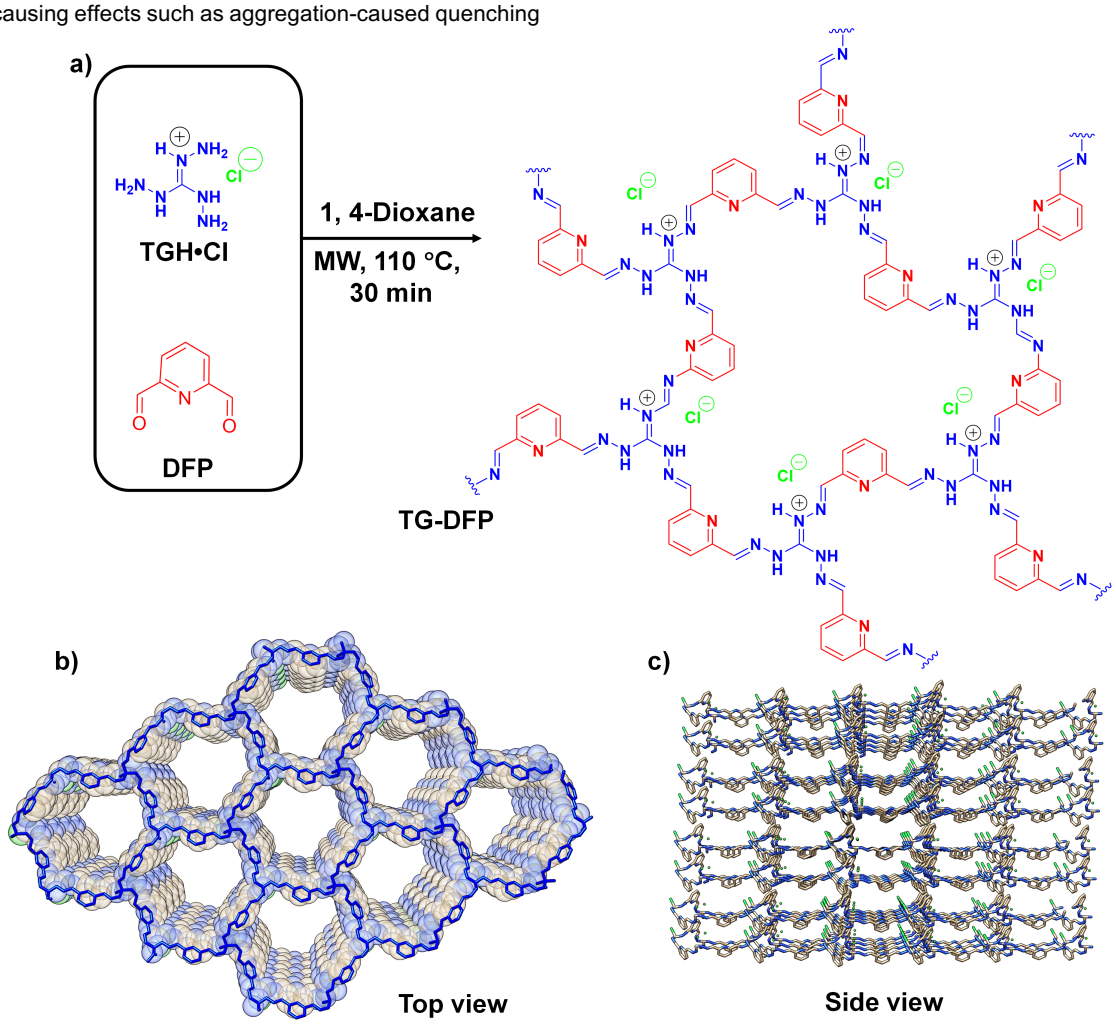

Figure 1. a) Schematic illustration for the synthesis of TG-DFP COF: (i) Microwave (MW) assisted synthesis in 1, 4-dioxane: H_2O (1: 1); Simulated crystal structure shown in a spacing filling/capped sticks eclipsed model in b) Top view and c) Side view, Cl^- ions were omitted for clarity.

To test our hypothesis, the guanidinium-based covalent organic framework (TG-DFP, Figure 1a) was obtained by the condensation of triamino-guanidinium hydrochloride salt (TGH•Cl) with diformylpyridine (DFP). The incorporation of guanidinium linkers into the iCOF backbone leads to multiple H-bonding sites within the framework. The H-bonding ability and the hydrophilic nature of TG-DFP iCOF offers several advantages, including improved water uptake, visible thermochromism, significant fluorescence enhancement under humid conditions or at low temperatures, and its potential use as a fluorescent chemosensor for trace amounts of water in organic solvents. Additionally, monitoring the complex structural changes caused by changes in humidity or temperature using conventional UV-Vis or spectrofluorometric methods poses a significant challenge.[21b, 23a, 24] In contrast to previous work reported on COF humidity[2a, 30] or temperature sensors,[25b, 26] our method for monitoring real-time structural alteration in response to change in humidity or temperature utilizes state-of-the-art operando UV-Vis[31] and operando FTIR techniques in DRIFTS mode,[32] providing superior accuracy.

Results and Discussion

Synthesis and Characterization

The formation of TG-DFP COF was confirmed by Fourier transform infrared (FT-IR) spectroscopy and solid-state ^{13}C nuclear magnetic resonance (^{13}C NMR) spectroscopy (Figure S1 and S2). The absence of the C=O stretching vibration band at 1723 cm^{-1} and appearance of a new band at 1629 cm^{-1} in the FT-IR spectra of TG-DFP COF provides confirmation of the formation of a -C=N bond. Additionally, the disappearance of the N-H stretching vibration band at 3185 cm^{-1}, which is associated with the amino group in TGH, serves as further evidence of the formation of an imine bond. The solid-state ^{13}C NMR spectrum (Figure S2) of TG-DFP COF also exhibited a peak at 165 ppm, indicative of the carbon atoms within the -C=N bonds. To elucidate the crystal structure (Figure 1b) of the synthesized TG-DFP COF, powder X-ray diffraction (PXRD, Figure S3) analysis of the solid sample was recorded. The PXRD pattern agrees well with our previous results on TTA-DFP gel.[33] As shown in Figure S3, the experimental PXRD pattern of TG-DFP COF shows its first peak at 5.13°, which corresponds to the (200) plane. In the wide-angle region, the reflection at 2θ = 28.79° associated with the (003) plane corresponds to the adjacent π-π stacking of the 2D layers (Figure 1c). Using the self-consistent charge density functional tight-binding method (SCC-DFTB)[34] within DFTB+ 17.1,[35] we performed geometry optimization. The COF structure formed in the hexagonal space group P3, following a triangular sequence arrangement. The unit cell parameters were determined as follows: a = 37.273 Å, b = 35.525 Å, and c = 12.30 Å. Compared to other reported hexagonal COFs, the observed PXRD pattern has relatively weak intensity. This phenomenon can be attributed to the electrostatic repulsion between the polar triaminoguanidinium units in the two layers and the intercalated chloride ions. This repulsion significantly hampers the organized π-π stacking over longer distances. This type of PXRD pattern is common in other guanidinium-based COFs previously documented.[36] The morphology of TG-DFP COF was studied by scanning electron microscopy (SEM, Figure S4), high-resolution transmission electron microscopy (HR-TEM, Figure S5), and atomic force microscopy (AFM, Figure S6). SEM, HR-TEM, and AFM images show that TG-DFP COF, as a powder, has a sheet-like morphology (Figure 2a-d, Figure S4-S6). High-magnification HR-TEM images confirm the presence of ordered and oriented crystal lattice fringes within the TG-DFP COF. This phenomenon is attributed to the stacked 2D layers with a stacking distance of 0.37 nm (Figure 2c), with the π-π stacking spacing closely matching the experimental wide-angle PXRD data. A thorough examination of the AFM images (Figure 2d and Figure S6) revealed that the thickness of the TG-DFP nanosheets is about 26 nm (as shown in Figure 2d), indicating the presence of a COF network consisting of multiple layers of stacked sheets.

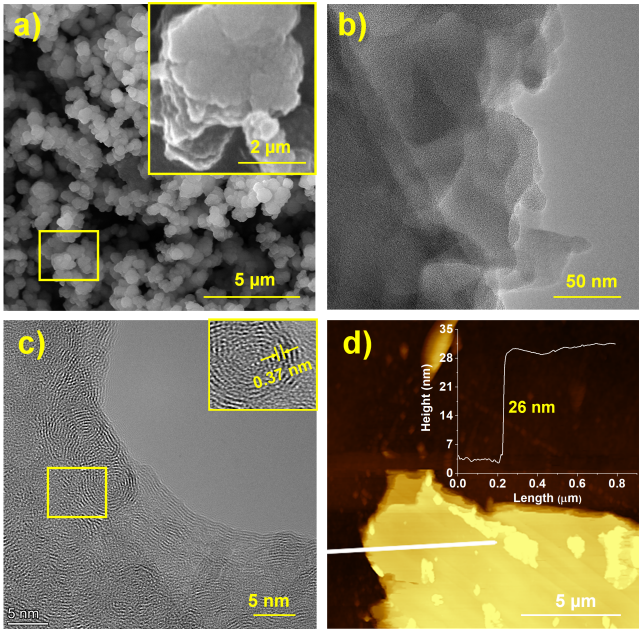

Figure 2. Microscopic analysis of TG-DFP COF: a-c) SEM and HRTEM images of TG-DFP COF at different magnifications (in c, inset displays the lattice fringes). d) AFM images of powder (inset displays the height profile).

Thermochromism in TGDFP COF:

As synthesized, TGDFP COF has a visibly yellow color. Once heated to 100 °C, the COF material showed a drastic and clearly visible color change from yellow to deep red (Figure 3a). When the sample is cooled at ambient temperature, the original color returned, changing from red-to-yellow. The reversible color change in response to temperature is attributed to the adsorption and desorption of water trapped in the COF network. To confirm this phenomenon, water adsorption studies were conducted. The water vapor adsorption characteristics of TG-DFP COF were evaluated using a IGAsorp vapor sorption analyser from Hiden, Isochema. The water vapor adsorption behaviour of the fully activated TG-DFP COF material exhibits a type I isotherm, (Figure 3b), with a maximum water uptake capacity of 23 wt% at RH = 98% and T = 298 K, which is comparable to recently reported water-adsorbing porous COFs.[30, 36c, 37] In addition, the water desorption curve is governed by a moderate hysteresis and incomplete desorption upon reducing the relative humidity to 0%, where 4% of water uptake is retained by the COF with a total working capacity of 18.7 wt% (Figure S7). The observed hysteresis reflects the relatively strong interaction between the framework and the free and intermediate water molecules that preferentially desorb[38] whereas, the un-desorbed water molecules signify the presence of the more polar guanidinium sites. The occupied sites are further verified by the second and the third cycles, collected at equilibrium, where we observe a full desorption of the water adsorbed with a total working capacity of 18 wt%. To understand the mechanism of the thermochromic color change, *operando* optical diffuse-reflectance (DRUV-DRIFTS) spectroscopic measurements (Figure 3c-d, Figure S8-9) were performed. The synthesized COF showed a π-π* CT absorption at λ_{max} = 494 nm. Upon incremental heating of the sample, this band was batho- and hyper-chromically shifted (50

nm), leading to an intense absorption band centered at λ_{max} = 553 nm. Moreover, the band gap of TG-DFP COF at 100 °C (ΔE = 1.83 eV, calculated from the Tauc plot, Figure S10) is lower than that of the COF at 25 °C (ΔE = 2.22 eV, Figure S10). The temperature-induced color changes were fully reversible with no significant colour bleaching observed after four consecutive cycles (Figure S11).

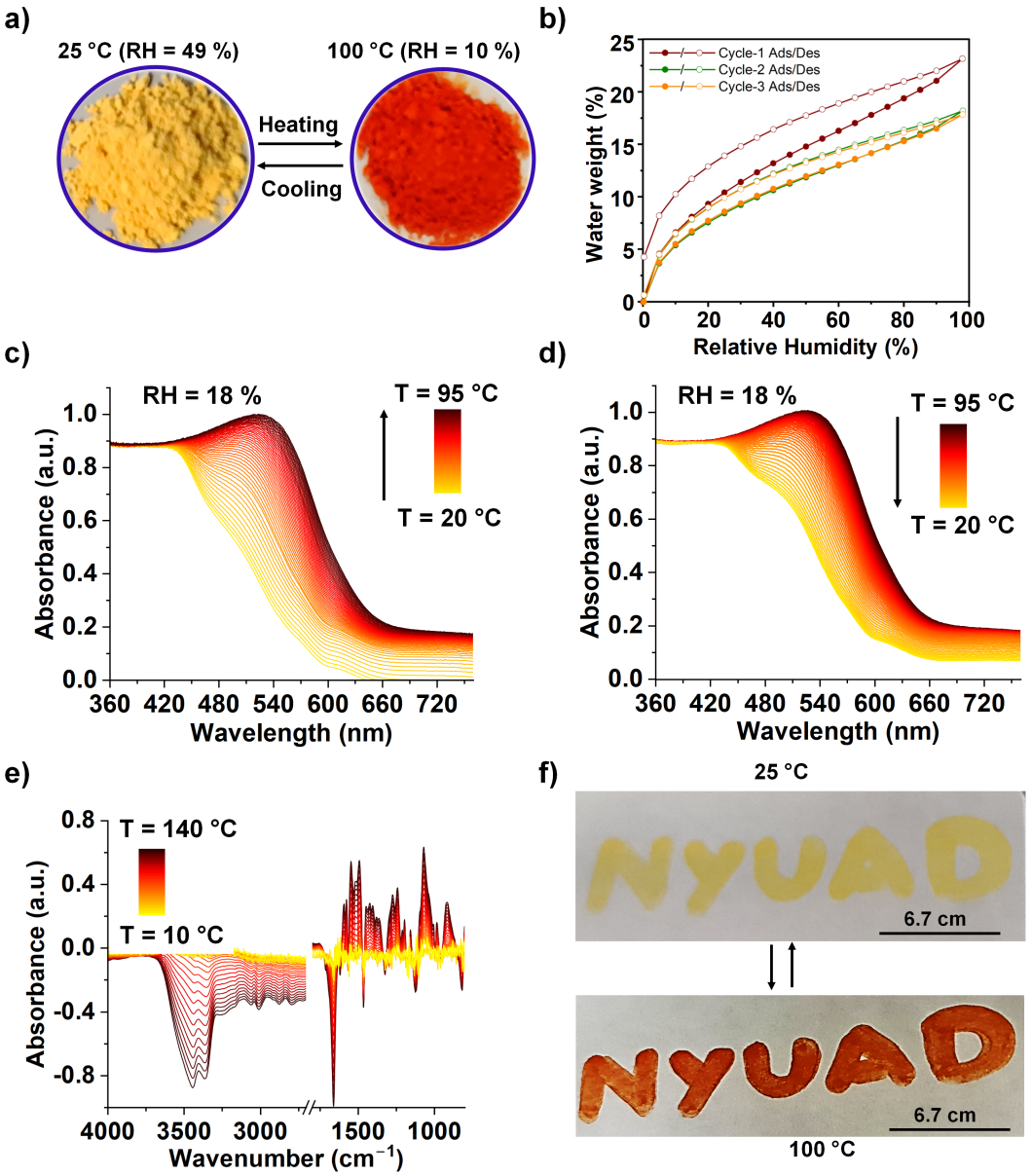

Figure 3. Analysis of versatile reversible thermochromic properties: a) Photographs of TG-DFP COF powder at temperatures of 25 and 100 °C (under different humidity conditions); b) Dynamic vapor sorption (DVS) isotherm of TG-DFP COF powder at 298K; c-d) *operando* diffuse-reflectance (DRUV) spectroscopic investigations of TG-DFP COF at different temperatures under constant RH flow (RH=18 %), the temperature interval is 1.5°C between spectra; e) Evolution of the FTIR spectra of TG-DFP COF recorded versus the temperatures under dry argon flow (spectra subtracted from the spectrum of the sample collected at different temperatures, the temperature interval is 4.5°C between spectra; d) Digital images of optical handwriting on the Whatman 40 filter paper with thermochromic TG-DFP COF. The images depicted in the top and bottom views correspond to the paper strip exposed to temperatures of 25 °C and 100 °C, respectively.

This result clearly indicates the robustness of the iCOF structure towards exposure and changes in both moisture and temperature. The thermally induced color change is possibly associated with the reversible sorption of water molecules from the iCOF network, with water molecules playing a crucial role in thermochromism. To confirm this mechanism, we also recorded UV-VIS spectra at variable temperature under dry-argon flow. Interestingly, the color change was not reversible under Argon (Figure S12-13), confirming the role of coordinating waters on the observed thermochromism of the iCOF. To directly observe the effect of

temperature on water sorption, we performed a thermally programmed desorption analysis on TG-DFP iCOF in diffuse reflectance infrared Fourier transform (DRIFT) spectral mode (Figure 3e). From the analysis of DRIFT, it is evident that the prepared TG-DFP iCOF has a broad peak at 3378 cm^{-1}, which is due to hydrogen-bonded water molecules adsorbed within the framework. The proportional decrease of the intensity of this band with increases in temperature confirms the thermal desorption of water. At the thermochromic transition temperature (100 °C), this band disappears completely. The plot of the corresponding evolution of the water band area (Figure S14) as a function of temperature clearly confirms the gradual desorption of water in a similar temperature range than that observed in the thermochromism measurement. To quantitatively measure the coordinating waters within the COF network, thermal analyses (TG /DSC, Figure S15) were performed. Thermogravimetric analysis (TGA), as depicted in Figure S15, revealed a two-step weight loss pattern. The initial weight loss of 13.3% occurred between 37 to 106 °C (Figure S15a) and was attributed to the removal of weakly adsorbed water. Subsequently, a weight loss at 295 °C was observed, corresponding to the degradation of the framework. From the TGA analysis, we calculated that 39.2 water molecules are present per unit cell. DSC analysis reveals a large endothermic peak at 99.6 °C (ΔH = 680.2 J g^{-1}, Figure S15b), corresponding to the removal of water molecules that are bound to the COF network, this finding is further supported by the decreased intensity of the OH stretching vibration of hydrogen-bonded water molecules at higher temperatures (3378 cm^{-1}). To shed light on the electronic structure of TG-DFP, we performed TD-DFT calculations on the TG-DFP single layer fragment capped with Hydrogen atoms. All electronic structure calculations were carried out at the level of PBE/6-311G using the Gaussian16 programme.[39] The choice of PBE[40] functional and basis sets 6-311G[41],[42] is based on a previous study that showed experimentally consistent HOMO- LUMO energy gaps[43] for a similar framework. To elucidate the hydration effect, we incorporated the implicit continuum solvation model to mimic non-specific binding of water molecules (dielectric constant was used here for pure water) to the framework. In addition, to account for specific binding consistent with experimental observation, we explicitly position a water molecule close to the guanidine subunit. The optimized geometries and their corresponding orbitals are shown in Figure 4. Our calculations indicated that the HOMO orbitals mostly lie on the pyridine ring, whereas LUMO orbitals are localized over the guanidine subunit. The computed HOMO-LUMO gap of 2.114 eV agrees reasonably well with our experimental value 1.83 eV. In addition, we found that the computed HOMO-LUMO gap in presence of water is larger than the gas phase (Figure 4a vs 4b) which supports our observation of the red shift in the absorption spectra upon heating (Figure 3c-d). To understand the changes in the charge distribution, we computed the difference in electron density between the ground *S0* and first excited single *S1* states (Figure S16). We observed a significant depletion of electron density on the guanidine subunit, accompanied by an increase in electron density on the pyridine ring during the excitation process. Consequently, our analysis suggests a substantial charge transfer character in the lowest energy optical transition. To access temperature dependance on the HOMO and LUMO orbitals we adopted a similar approach previously used.[43] We performed molecular dynamics simulations at three different temperatures 293, 325, and 363 K using a semi empirical and tight binding quantum mechanical method xTB-GFN2 and with implicit water as solvent. All MD simulations were performed for 10 ps with a time step of 2 fs using xTB tight binding platform. From the MD trajectory, we extracted the structure close to the mean RMSD and computed the HOMO-LUMO orbitals at the level of PBE/6-311G using the Gaussian16 program.[39] Figure S17 shows the HOMO-LUMO orbitals and the corresponding energy gaps at three different temperatures. We observed that the HOMO-LUMO gaps decreases with increase temperature and agree qualitatively with the experimental observations of the redshift in the absorption spectra.

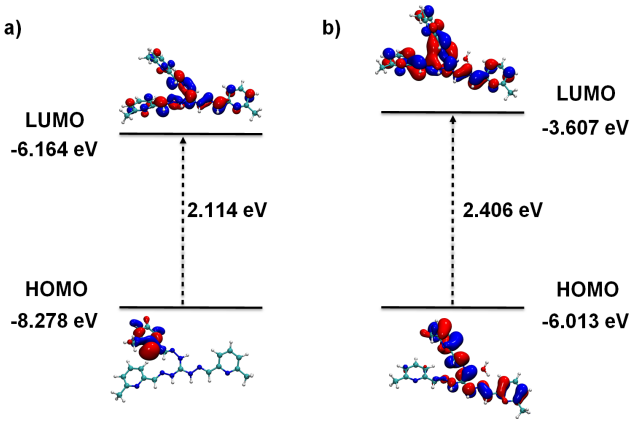

Figure 4. a-b) 3D-isosurface plots for single layer fragment, in gas phase and aqueous solution respectively.

To verify any structural changes at the thermochromic transition temperature, we recorded PXRD at several temperatures from 30 ° C to 100 °C, concentrating on the wide-angle region. The raw diffraction profiles at two representative temperatures, 35 °C and 100 °C, are shown in Figures S18. At all temperatures, the pattern remained the same, exhibiting primarily two diffuse peaks centered at spacings 0.42 nm (Peak 1) and 0.34 nm (Peak 2), with no significant temperature dependence (Figure S18a-b). While the peak width and peak intensity are essentially thermally invariant for Peak1 (Figures S19a-c), substantial increases and large decreases were seen for the width and intensity, respectively, for Peak 2. The spacings proved not to be temperature dependent, even up to 100 °C, an indicator that the crystal structure remained intact, while the behavior of the width and the intensity (seen for Peak 2) clearly indicated that the extent of correlation notably weakens with increasing temperature. To check the stability of the thermally treated TG-DFP COF, we performed ^{13}CPMAS NMR (Figure S20). No significant changes in NMR signals were observed upon thermal treatment, clearly indicating stability under extreme conditions. Interestingly, due to the high hydrophilicity of TG-DFP COF, the material disperses well in water without aggregating. The homogeneously dispersed solution was used as a thermochromic ink for optical labeling of a low-cost filter paper (Figure 3f). When thermally heated, the handwritten letters (NYUAD) undergo a distinct color change. The

paper strip coated with the iCOF is easily folded/portable and can be regenerated after several rounds of thermal annealing. (Supporting video s1).

Fluorescent hydrochromic behavior of TGDFP COF:
To investigate the effect of temperature on luminescence (Figure 5a), the solid-state luminescence of TG-DFP COF was measured at a wide range of temperatures (–15 °C to 105 °C, Figure S21). It is a great challenge to design and develop materials that exhibit luminescence enhancement under extreme conditions while maintaining their inherent properties. Interestingly, at –15 °C, the powder TG-DFP emits a strong

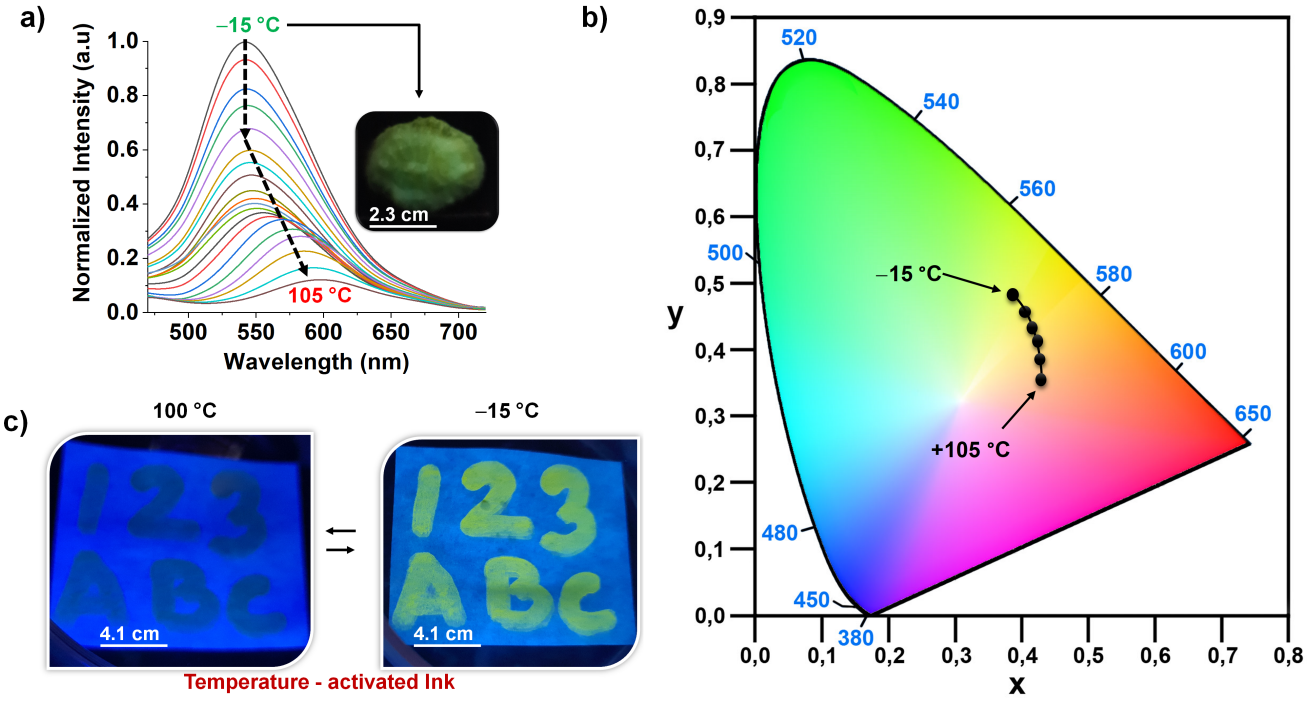

Figure 5. Fluorescence thermo/hydrochromism: a) Variable temperature solid-state fluorescence spectra (λ_{ex} = 365 nm) from TG-DFP iCOF heating under air in the wide range of temperature; b) CIE coordinates corresponding to the emission color observed at each temperature; c) Images of a filter paper strip coated with fluorescent TG-DFP COF showing its thermos/hydrochromic fluorescence response before and after exposure to two different temperatures under a UV lamp (365 nm).

yellow fluorescence (λ_{em} = 550 nm, Figure 5a, inset) under excitation with a 375 nm light, which is due to charge transfer from the DFP to the guanidinium moiety (TGH^+).[21a] Although the monomers DFP and TGH^+ are non-emissive, the TG-DFP COF is highly emissive at very low temperatures. At low temperatures, the reduced molecular motion within the iCOF networks stabilizes the hydrogen bonds.[14j, 44] This stabilization in turn, can lead to a reduction in non-radiative relaxation pathways,[28-29] thereby promoting radiative processes that lead to a remarkable increase in emission intensity. When the temperature isf increased gradually, the weak H-bonds are disrupted, the emission intensity decreases dramatically, and a large bathochromic shift of emission maximum (λ_{em} = 550 nm) occurs. This large hypo/bathochromic shifts can be detected visually. The chromaticity coordinate (CIE) also shows a large degree of color change in the solid-state in the temperature range of –15°C to 105 °C (Figure 5b, Table S1). The hypochromic shift at high temperature is due to the disruption of H-bonds as the temperature increases. Moreover, upon cooling the sample, the yellow emission is regenerated, showing the reversible thermofluorochromic behavior of the COF (Figure S22). The TG-DFP COF material can further be used for smart anticounterfeiting applications, the handwritten letters (Figure 5c) and numbers on a commercial filter paper showed a bright yellow emission at low temperature and the emission intensity of the pattern quenches instantaneously upon heating. The reason we only measure down to -15°C is that the instrument we used for the luminescence study is not capable of operating below –15°C. However, the luminescence could be enhanced below –15°C. To investigate this phenomenon, we applied a coating of TG-DFP COF material to Whatman 40 filter paper and immersed it in liquid nitrogen. The TG-DFP COF coated paper showed a pronounced luminescent emission at cryogenic temperatures (see Video 2, Figure S23).

TG-DFP COF as an Optical hygro-sensor: Next, we tested the humidity-dependent optical properties at constant temperature (25 ºC) and humidity between 0 and 20% of RH. The activated TGDFP-COF showed an absorption onset at 530 nm (Figure 6a). As shown by diffuse reflectance spectroscopy (DRS), the band decreases significantly with the increase of RH in the range of 0-20 RH%, while no detectable change was observed at values higher than 20 RH% (Figure 6b). Figure 6c shows how the optical density of TGDFP-COF changes as a function of humidity. As the

RH increases, the optical density decreases. In addition, we also investigated the effects of humidity on the photoluminescence of TG-DFP COF in the solid state. As shown in Figure 6d, TG-DFP COF shows an enhancement of fluorescence in response to an increase in humidity from ~10 to ~90 RH% for excitation at 375 nm. In response to the high humidity (RH = 90%), the COF material showed a significant change in emission color (inset Figure 6e). The plot of emission intensity as a function of RH shows a nonlinear relationship over the entire RH range (Figure 6e). The different impacts of humidity on the absorption and photoluminescence of the COF material can be attributed to the distinct ways in which moisture interacts with the material's electronic and structural properties. For example, swelling due to moisture absorption can alter the structural integrity of COFs. This change may not greatly affect the electronic transitions responsible for absorption. However, the same structural changes can have a more profound effect on the processes that govern photoluminescence, such as the alignment of energy levels and the efficiency of electron-hole pair recombination. Other factors can be related to the competition of radiative and non radiative pathways, solvation of the excited states and/or variation of the refractive index under various conditions.

For applications in daily life, such as the production of responsive textiles, we synthesized TG-DFP COF in the presence of cotton fabric (2 cm × 2cm). The obtained cotton fabric was uniformly covered with the TG-DFP material. The composite showed excellent reversible response to moisture, which is visually detectable (Figure 6f). At high humidity (RH = 90%), the color of the cotton fabric is light yellow and slowly changes to red when heated in a temperature-controlled oven at 80 °C, decreasing RH

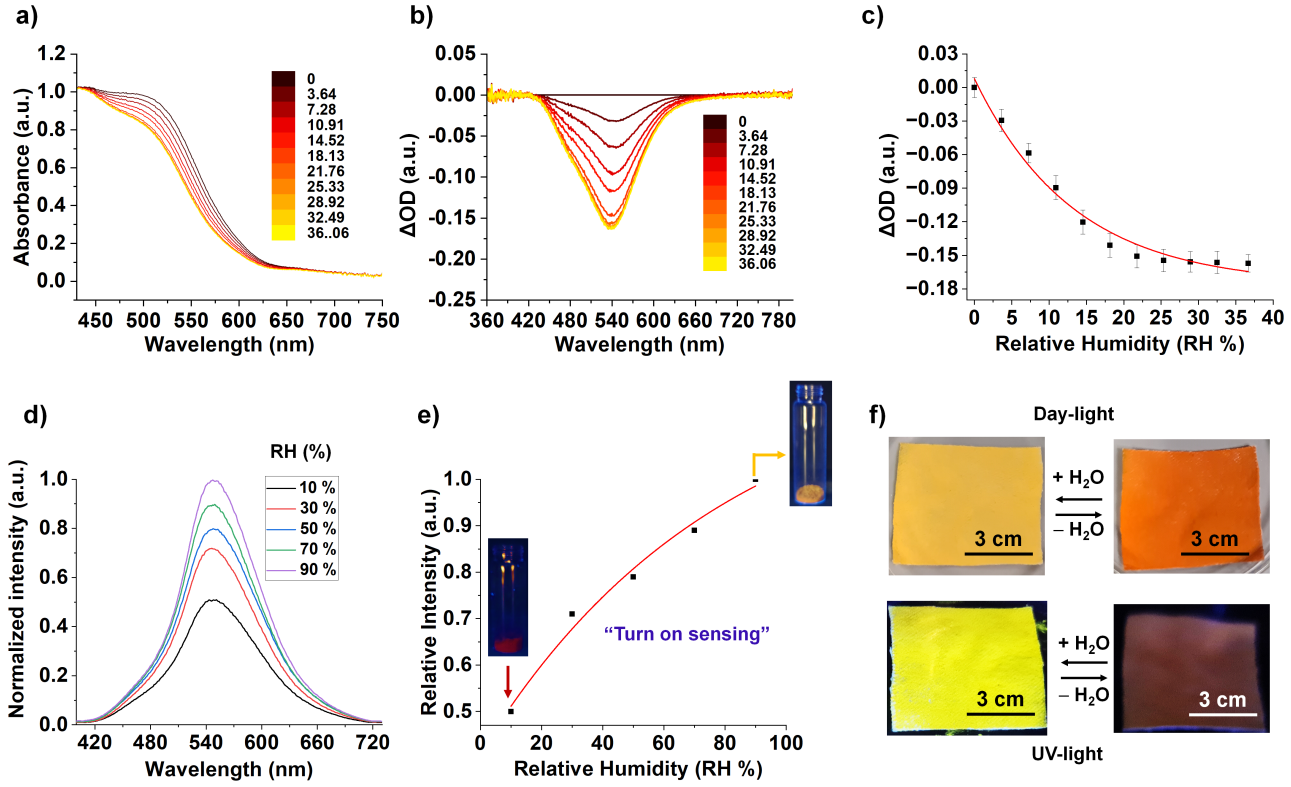

Figure 6. Solid-state Humidity sensing: a) Solid-state, diffuse reflectance spectra (DRS) of TG-DFP COF at different humidity level; b) Humidity dependence of optical density measured on TG-DFP COF; c) Plot of the absorbance band at 530 nm as a function of different RH percentages (RH%); d) Humidity-dependent emission spectra of TG-DFP COF after exposure to different RHs (inset: photographs of TG-DFP COF powder under different humid conditions under a 365 nm UV-lamp); e) linear plot of fluorescence intensity as a function RH; c) Dynamic vapor sorption (DVS) isotherm of TG-DFP COF powder at 298K; f) Optical images of the reversible color change in day-light (top) and under UV light (bottom panel) of a cotton fabric coated with TG-DFP COF powder between humid and dry air.

from 90% to 10% (Figure 6f). Under UV light, the fabric shows a rapid and reversible fluorescent color change. Under humid conditions, the COF-coated fabric shows bright yellow fluorescence (Figure 6f, top panel), but in dry atmosphere, the fabric is almost non-emissive (Figure 5f, bottom panel). Overall, our TG-DFP COF has the potential to be an effective platform for developing rapid and reversible RH sensing system with remarkable stability. The color changes of the cotton fabric are primarily determined by the relative humidity or a combination of temperature and humidity. In Figure 6f, we heated the COF-coated fabric at 100 °C in an open atmosphere and the color change was reversible. However, after we activated the fabric at 100 °C and then placed it in a glove box, the color change was irreversible under glove box controlled atmosphere (nitrogen). This observation confirms the influence of adsorbed water from atmospheric humidity on the observed thermochromism of the iCOF. We have now provided evidence for this observation in the revised Figure S24.

TG-DFP COF for Visual Water Sensing Applications in Organic Solvent:

The enhancement of luminescence caused by water prompted us to quantify trace amounts of water in organic solvents. The detection of water in THF was tested by gradually increasing the water content in 3 mL of THF containing 5 mg of TG-DFP COF as suspension. When the water content was increased up to 0.8 wt.% (v/v), a significant increase in emission intensity was observed, accompanied by a slight blue shift in the emission spectra to lower wavelengths (Figure 7a). When a trace of water is added to TG-DFP COF, dispersed in THF, the excited state lifetime value increases from 0.28 ns to 0.48 ns (Figure 7b), clearly indicating that there is a significant interaction between the framework and the water molecules. The detection limit for water is 0.03 wt.% (v/v) (Figure 7c), which is sufficient for detecting trace amounts of residual water in dry solvents. We assume that the iCOF network in dry THF is fully saturated with the organic solvent. Upon gradual addition of water, the water molecules displace the THF molecules, leading to the formation of hydrogen bonds with the guanidinium linker throughout the network. This displacement reduces the non-radiative pathway and eventually increases the emission intensity. Unlike conventional COFs used to detect water, our TG-DFP iCOF can detect trace amounts of water in organic solvents through a fluorescence "turn-on" mechanism. The distinct “turn-on” detection of moisture in organic solvents is of great importance for industrial applications.

To investigate the practical utility of the solid TG-DFP iCOF material, we fabricated several iCOF-supporting test strips from commercially available Whatman filter paper. After immersing these strips in THF solutions containing different amounts of water (0–0.8% v/v) and illuminating the paper strips with 365 nm UV light, an abrupt color change can be seen when the COF strip is exposed to an increasing amount of water (Figure 7d). To test the reusability of the sensor, we heated the wet paper strip with a heat gun, and its fluorescent color was restored. These results suggest that the COF-coated paper strip could serve as an efficient and recyclable portable water sensor. For reusability of the TG-DFP coated COF paper strip, we subjected the paper strip to heating at 100 °C for 1 minute inside a glass vial (Figure S25). Further, the PXRD data of the regenerated COF powder isolated by scratching the iCOF-coated filter paper were subsequently recorded and show identical patterns to the original TG-DFP iCOF (Figure S26).

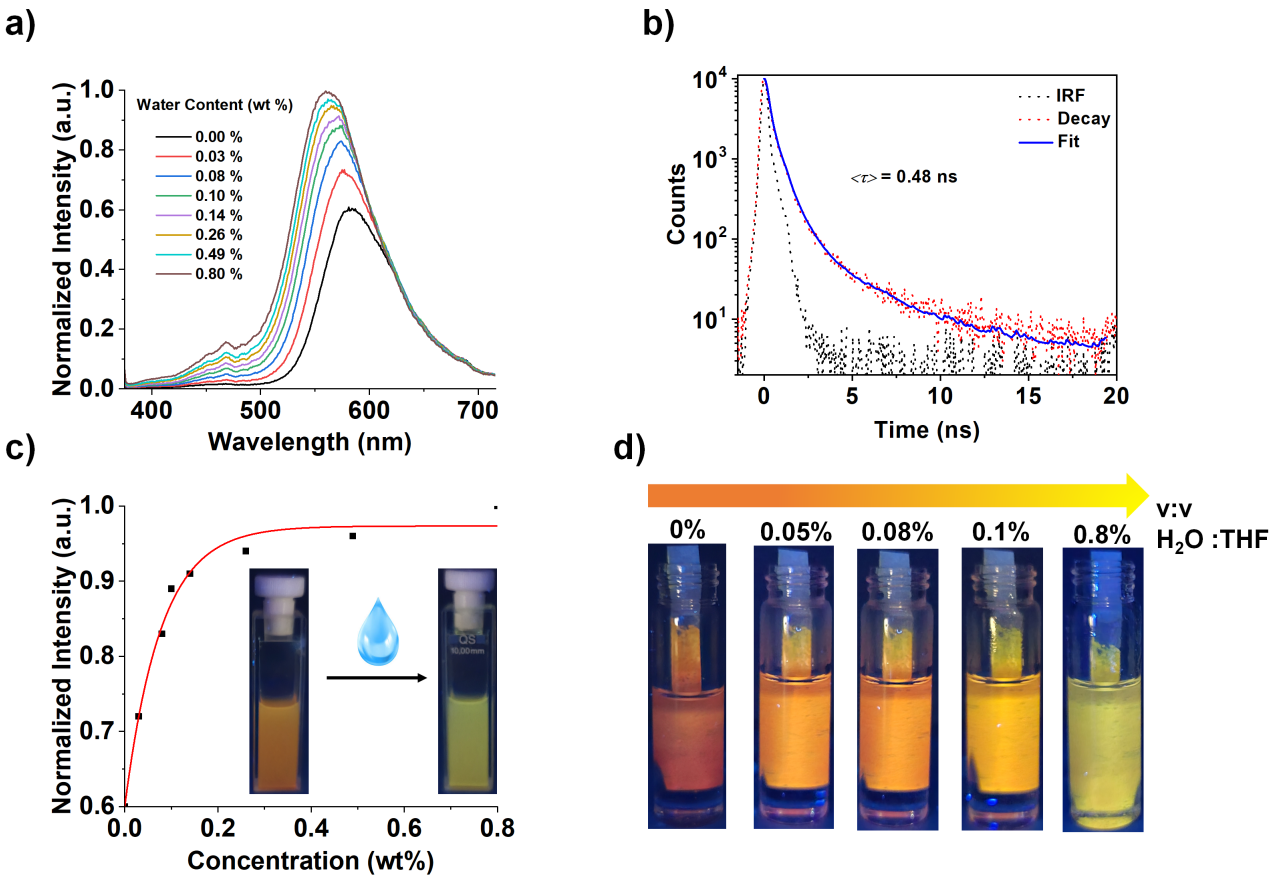

Figure 7. a) Emission spectral change in stirred suspension of activated TG-DFP COF in dry THF upon incremental addition of aliquots of water (% v/v); b) Fluorescence decay profile of TG-DFP COF in THF after addition of water; c) Non-linear fitting curve of fluoresce intensity against different concentrations of water content; d) Photographs showing ratiometric fluorescence color change of the activated TG-DFP COF coated test strip when exposed to THF solutions containing different amounts of water (0-0.8 wt %).

Conclusion

In summary, we have successfully developed a strategy to enhance the optical and photoluminescent properties of ionic COFs in the solid state by limiting the nonradiative transitions through the incorporation of a H-bonding guanidinium building block. The optical and fluorescent response can be reversibly modulated by the presence of adsorbed water molecules in the iCOF channels. Unlike conventional single-function COF sensors, our strategically designed TG-DFP iCOF sensor offers ultra-fast sensitivity and dual functionality. It serves as a responsive system that can monitor both temperature and humidity simultaneously, under constant humidity and temperature, respectively. Interestingly, our iCOF material shows changes in its fluorescence spectral properties over a wide temperature range, especially below room temperature. The fluorescence properties at temperatures below room temperature have not been studied for any other COF material. Due to the ease of preparation of our iCOF and the rapid optical response, we have developed a portable COF-coated test strip made of plain paper. This test strip is capable of visualizing extremely low water content (0.03% v-v) in organic solvents. This work provides a unique route to the development of a multifunctional, color-tunable fluorescence, and optical iCOFs-based sensor for humidity and temperature.

Supporting Information

The authors have cited additional references within the Supporting Information.

Acknowledgements

This work was supported by New York University Abu Dhabi and the NYUAD Water Research Center, funded by Tamkeen under the NYUAD Research Institute Award (project CG007). We thank NYUAD for their generous support for the research program. We thank Sandooq Al Watan (Grant No. SWARD-S22-014, Project ID: PRJ-SWARD-628) for their generous support. The research work was carried out by using the Core Technology Platform resources at NYUAD. M.A. acknowledges support from EPSRC, EP/S015868/1, and HPC resources on Thomas via the Materials Chemistry Consortium, EP/P020194. M. El-Roz acknowledges the Normandy Region and the European union for financial support (project SuntoChem). F.C. and N.S. acknowledge support from UAE University (Grant# 12S106).

Keywords: Ionic COF • Humidity Sensing • Temperature Sensing • Solid state • Detection of water

[1] a) M. De Bastiani, M. I. Saidaminov, I. Dursun, L. Sinatra, W. Peng, U. Buttner, O. F. Mohammed, O. M. Bakr, *Chem. Mater.* **2017**, *29*, 3367-3370; b) M. Dharmarwardana, B. M. Otten, M. M. Ghimire, B. S. Arimilli, C. M. Williams, S. Boateng, Z. Lu, G. T. McCandless, J. J. Gassensmith, M. A. Omary, *PNAS* **2021**, *118*, e2106572118; c) Y. Gao, P. Jing, N. Yan, M. Hilbers, H. Zhang, G. Rothenberg, S. Tanase, *Chem. Commun.* **2017**, *53*, 4465-4468; d) L. Tom, M. R. P. Kurup, *J. Mater. Chem. C* **2020**, *8*, 2525-2532; e) B.-X. Li, Z. Luo, W.-G. Yang, H. Sun, Y. Ding, Z.-Z. Yu, D. Yang, *ACS Nano* **2023**, *17*, 6875-6885; f) W. Zhang, X. Huang, W. Liu, Z. Gao, L. Zhong, Y. Qin, B. Li, J. Li, *ACS Appl. Mater. Interfaces* **2023**, *15*, 4469-4476.

[2] a) S. Jhulki, A. M. Evans, X.-L. Hao, M. W. Cooper, C. H. Feriante, J. Leisen, H. Li, D. Lam, M. C. Hersam, S. Barlow, J.-L. Brédas, W. R. Dichtel, S. R. Marder, *JACS* **2020**, *142*, 783-791; b) H. S. Jung, P. Verwilst, W. Y. Kim, J. S. Kim, *Chem. Soc. Rev.* **2016**, *45*, 1242-1256; c) P. Kumar, R. Sakla, A. Ghosh, D. A. Jose, *ACS Appl. Mater. Interfaces* **2017**, *9*, 25600-25605; d) Y.-J. Gao, G. Romolini, H. Huang, H. Jin, R. A. Saha, B. Ghosh, M. De Ras, C. Wang, J. A. Steele, E. Debroye, J. Hofkens, M. B. J. Roeffaers, *J. Mater. Chem. C* **2022**, *10*, 12191-12196; e) W. Huang, Y. Jiang, X. Li, X. Li, J. Wang, Q. Wu, X. Liu, *ACS Appl. Mater. Interfaces* **2013**, *5*, 8845-8849.

[3] a) M. Chen, Y. He, H. Liang, H. Zhou, X. Wang, X. Heng, Z. Zhang, J. Gan, Z. Yang, *ACS Photonics* **2022**, *9*, 1415-1424; b) Z. Duan, Y. Jiang, H. Tai, *J. Mater. Chem. C* **2021**, *9*, 14963-14980; c) F. Güder, A. Ainla, J. Redston, B. Mosadegh, A. Glavan, T. J. Martin, G. M. Whitesides, *Angew. Chem., Int. Ed.* **2016**, *55*, 5727-5732; d) Q. Hua, J. Sun, H. Liu, R. Bao, R. Yu, J. Zhai, C. Pan, Z. L. Wang, *Nat. Commun.* **2018**, *9*, 244.

[4] a) Z. Zhang, T. Lu, D. Yang, S. Lu, R. Cai, W. Tan, *Small* **2022**, *18*, 2203334; b) L. Zhou, J.-F. Liao, Z.-G. Huang, J.-H. Wei, X.-D. Wang, W.-G. Li, H.-Y. Chen, D.-B. Kuang, C.-Y. Su, *Angew. Chem., Int. Ed.* **2019**, *58*, 5277-5281; c) S. Miho, T. Fumoto, Y. Mise, K. Imato, S. Akiyama, M. Ishida, Y. Ooyama, *Mater. Adv.* **2021**, *2*, 7662-7670; d) S. Rauf, M. T. Vijjapu, M. A. Andrés, I. Gascón, O. Roubeau, M. Eddaoudi, K. N. Salama, *ACS Appl. Mater. Interfaces* **2020**, *12*, 29999-30006; e) K. Szendrei, A. Jiménez-Solano, G. Lozano, B. V. Lotsch, H. Míguez, *Adv. Opt. Mater.* **2017**, *5*, 1700663; f) H.-Q. Yin, J.-C. Yang, X.-B. Yin, *Anal. Chem.* **2017**, *89*, 13434-13440; g) A. Zadehnazari, A. Khosropour, A. A. Altaf, S. Amirjalayer, A. Abbaspourrad, *Adv. Opt. Mater.* **2023**, *11*, 2300412; h) X. Zhai, P. Feng, N. Song, G. Zhao, Q. Liu, L. Liu, M. Tang, Y. Tang, *Inorg. Chem. Front.* **2022**, *9*, 1406-1415; i) L. Zhan, Y. Tang, W. Ning, G. Xie, C. Zhong, S. Gong, C. Yang, *J. Chem. Eng.* **2023**, *454*, 140182.

[5] A. Theodosiou, P. Savva, E. Mendoza, M. F. Petrou, K. Kalli, *IEEE Sens. J.* **2021**, *21*, 16086-16092.

[6] H. Singh, V. K. Tomer, N. Jena, I. Bala, N. Sharma, D. Nepak, A. De Sarkar, K. Kailasam, S. K. Pal, *J. Mater. Chem. A* **2017**, *5*, 21820-21827.

[7] S. Gopalakrishnan, J. Waimin, A. Zareei, S. Sedaghat, N. Raghunathan, A. Shakouri, R. Rahimi, *Sci. Rep.* **2022**, *12*, 8011.

[8] R. Das, S. Bej, H. Hirani, P. Banerjee, *ACS Omega* **2021**, *6*, 14104-14121.

[9] a) W. Jeong, J. Song, J. Bae, K. R. Nandanapalli, S. Lee, *ACS Appl. Mater. Interfaces* **2019**, *11*, 44758-44763; b) L. Ma, R. Wu, A. Patil, S. Zhu, Z. Meng, H. Meng, C. Hou, Y. Zhang, Q. Liu, R. Yu, J. Wang, N. Lin, X. Y. Liu, *Adv. Funct. Mater.* **2019**, *29*, 1904549.

[10] J. Lee, *Macromol. Biosci.* **2005**, *5*, 1085-1093.

[11] T. Delipinar, A. Shafique, M. S. Gohar, M. K. Yapici, *ACS Omega* **2021**, *6*, 8744-8753.

[12] a) N. Herzer, H. Guneysu, D. J. D. Davies, D. Yildirim, A. R. Vaccaro, D. J. Broer, C. W. M. Bastiaansen, A. P. H. J. Schenning, *JACS* **2012**, *134*, 7608-7611; b) X. Yu, X. Ge, L. Geng, H. Lan, J. Ren, Y. Li, T. Yi, *Langmuir* **2017**, *33*, 1090-1096.

[13] a) V. Montes-García, P. Samorì, *Adv. Mater*, *n/a*, 2208766; b) M. A. Squillaci, X. Zhong, L. Peyruchat, C. Genet, T. W. Ebbesen, P. Samorì, *Nanoscale* **2019**, *11*, 19315-19318.

[14] a) U. Mogera, A. A. Sagade, S. J. George, G. U. Kulkarni, *Sci. Rep.* **2014**, *4*, 4103; b) M. A. Squillaci, L. Ferlauto, Y. Zagranyarski, S. Milita, K. Müllen, P. Samorì, *Adv. Mater* **2015**, *27*, 3170-3174; c) S. Samai, C. Sapsanis, S. P. Patil, A. Ezzeddine, B. A. Moosa, H. Omran, A.-H. Emwas, K. N. Salama, N. M. Khashab, *Soft Matter* **2016**, *12*, 2842-2845; d) S.-H. Hwang, D. Kang, R. S. Ruoff, H. S. Shin, Y.-B. Park,

ACS Nano **2014**, *8*, 6739-6747; e) Y. Ma, X. Hu, S. Li, Y. He, Z. Xia, K. Cai, *Macromol Mater Eng* **2022**, *307*, 2100686; f) R. Lan, W. Shen, W. Yao, J. Chen, X. Chen, H. Yang, *Mater. Horiz.* **2023**, *10*, 2824-2844; g) Z. Sun, Z. Wang, Y. Ni, L. Xi, L. M. Roch, H. F. Nour, M. A. Olson, *Chem. Commun.* **2021**, *57*, 6554-6557; h) Z. Sun, Y. Ni, T. Prakasam, W. Liu, H. Wu, Z. Zhang, H. Di, K. K. Baldridge, A. Trabolsi, M. A. Olson, *Chem. Eur. J.* **2021**, *27*, 9360-9371; i) H. F. Nour, T. El Malah, T. A. Khattab, M. A. Olson, *Mater. Today Chem.* **2020**, *17*, 100289; j) Y. Ni, Z. Sun, Y. Wang, H. F. Nour, A. C. H. Sue, N. S. Finney, K. K. Baldridge, M. A. Olson, *J. Mater. Chem. C* **2019**, *7*, 7399-7410; k) Y. Xu, T. Yuan, H. F. Nour, L. Fang, M. A. Olson, *Chem. Eur. J.* **2018**, *24*, 16558-16569; l) T. Yuan, Y. Xu, C. Zhu, Z. Jiang, H.-J. Sue, L. Fang, M. A. Olson, *Chem. Mater* **2017**, *29*, 9937-9945; m) T. Yuan, M. Vazquez, A. N. Goldner, Y. Xu, R. Contrucci, M. A. Firestone, M. A. Olson, L. Fang, *Adv. Funct. Mater.* **2016**, *26*, 8604-8612..

[15] a) C. Chakraborty, U. Rana, S. Moriyama, M. Higuchi, *ACS Appl. Polym. Mater.* **2020**, *2*, 4149-4159; b) S. Schoelch, J. Vapaavuori, F.-G. Rollet, C. J. Barrett, *Macromol. Rapid Commun.* **2017**, *38*, 1600582.

[16] a) S.-S. Bao, N.-Z. Li, J. M. Taylor, Y. Shen, H. Kitagawa, L.-M. Zheng, *Chem. Mater* **2015**, *27*, 8116-8125; b) J. M. Stangl, D. Dietrich, A. E. Sedykh, C. Janiak, K. Müller-Buschbaum, *J. Mater. Chem. C* **2018**, *6*, 9248-9257; c) H. Yu, C. Wang, F. Meng, J. Xiao, J. Liang, H. Kim, S. Bae, D. Zou, E.-S. Kim, N.-Y. Kim, M. Zhao, B. Li, *Carbon* **2021**, *183*, 578-589; d) A. Karmakar, P. G. M. Mileo, I. Bok, S. B. Peh, J. Zhang, H. Yuan, G. Maurin, D. Zhao, *Angew. Chem., Int. Ed.* **2020**, *59*, 11003-11009; e) Z. Du, F. Zhang, H. Lin, W. Guo, M. Tian, K. Yu, D. Gao, F. Qu, *ACS Appl. Mater. Interfaces* **2023**, *15*, 10064-10074; f) M. Yang, S.-Q. Wang, Z. Liu, Y. Chen, M. J. Zaworotko, P. Cheng, J.-G. Ma, Z. Zhang, *JACS* **2021**, *143*, 7732-7739.

[17] L. Chen, J.-W. Ye, H.-P. Wang, M. Pan, S.-Y. Yin, Z.-W. Wei, L.-Y. Zhang, K. Wu, Y.-N. Fan, C.-Y. Su, Nat. Commun. **2017**, *8*, 15985.

[18] a) S. Zuluaga, E. M. A. Fuentes-Fernandez, K. Tan, F. Xu, J. Li, Y. J. Chabal, T. Thonhauser, *J. Mater. Chem. A* **2016**, *4*, 5176-5183; b) P. M. Schoenecker, C. G. Carson, H. Jasuja, C. J. J. Flemming, K. S. Walton, Ind. Eng. Chem. Res. **2012**, *51*, 6513-6519; c) M. J. Kalmutzki, C. S. Diercks, O. M. Yaghi, *Adv. Mater* **2018**, *30*, 1704304.

[19] a) L. Guo, L. Yang, M. Li, L. Kuang, Y. Song, L. Wang, *Coord. Chem. Rev.* **2021**, *440*, 213957; b) T. Skorjanc, D. Shetty, M. Valant, *ACS Sensors* **2021**, *6*, 1461-1481; c) G. Das, B. P. Biswal, S. Kandambeth, V. Venkatesh, G. Kaur, M. Addicoat, T. Heine, S. Verma, R. Banerjee, *Chem. Sci.* **2015**, *6*, 3931-3939.

[20] a) J. Dong, K. Zhang, X. Li, Y. Qian, H. Zhu, D. Yuan, Q.-H. Xu, J. Jiang, D. Zhao, *Nat. Commun.* **2017**, *8*, 1142; b) P. Albacete, A. López-Moreno, S. Mena-Hernando, A. E. Platero-Prats, E. M. Pérez, F. Zamora, *Chem. Commun.* **2019**, *55*, 1382-1385; cH.-Q. Yin, F. Yin, X.-B. Yin, *Chem. Sci.* **2019**, *10*, 11103-11109; d) S.-Y. Ding, M. Dong, Y.-W. Wang, Y.-T. Chen, H.-Z. Wang, C.-Y. Su, W. Wang, *JACS* **2016**, *138*, 3031-3037.

[21] a) G. Das, B. Garai, T. Prakasam, F. Benyettou, S. Varghese, S. K. Sharma, F. Gándara, R. Pasricha, M. Baias, R. Jagannathan, N. i. Saleh, M. Elhabiri, M. A. Olson, A. Trabolsi, *Nat. Commun.* **2022**, *13*, 3904; b) W. Ma, S. Jiang, W. Zhang, B. Xu, W. Tian, Macromol. Rapid Commun. **2020**, *41*, 2000003. c) C. Wu, L. Xia, S. Xia, B. Van der Bruggen, Y. Zhao, *Small* **2023**, *19*, 2206041; d) Y. Zhao, N. Mamrol, W. A. Tarpeh, X. Yang, C. Gao, B. Van der Bruggen, *Prog. Mater. Sci.* **2022**, *128*, 100958.

[22] L. Ascherl, E. W. Evans, M. Hennemann, D. Di Nuzzo, A. G. Hufnagel, M. Beetz, R. H. Friend, T. Clark, T. Bein, F. Auras, *Nat. Commun.* **2018**, *9*, 3802.

[23] a) C. Guan, J. Cai, X. Liu, L. Guo, *Sens. Actuators B Chem.* **2022**, *355*, 131323; b) Y. Zhang, W. Zhang, Q. Li, C. Chen, Z. Zhang, *Sens. Actuators B Chem.* **2020**, *324*, 128733.

[24] a) L. Deng, X. Kang, T. Quan, L. Yang, S. Liu, K. Zhang, M. Gao, Z. Xia, D. Gao, *ACS Appl. Mater. Interfaces* **2021**, *13*, 33449-33463; b) H.-L. Qian, C. Dai, C.-X. Yang, X.-P. Yan, *ACS Appl. Mater. Interfaces* **2017**, *9*, 24999-25005; c) S. Jiang, L. Meng, W. Ma, G. Pan, W. Zhang, Y. Zou, L. Liu, B. Xu, W. Tian, *Mater. Chem. Front.* **2021**, *5*, 4193-4201.

[25] a) W. K. Haug, E. M. Moscarello, E. R. Wolfson, P. L. McGrier, *Chem. Soc. Rev.* **2020**, *49*, 839-864; b) L. Bourda, A. M. Kaczmarek, M. Peng, S. Mohanty, H. Rijckaert, P. Van Der Voort, K. Van Hecke, *ACS Appl. Mater. Interfaces* **2023**, *15*, 37696-37705; c) P. Zhang, S. Chen, C. Zhu, L. Hou, W. Xian, X. Zuo, Q. Zhang, L. Zhang, S. Ma, Q. Sun, *Nat. Commun.* **2021**, *12*, 1844.

[26] A. M. Kaczmarek, Y.-Y. Liu, M. K. Kaczmarek, H. Liu, F. Artizzu, L. D. Carlos, P. Van Der Voort, *Angew. Chem., Int. Ed.* **2020**, *59*, 1932-1940.

[27] A. M. Kaczmarek, H. S. Jena, C. Krishnaraj, H. Rijckaert, S. K. P. Veerapandian, A. Meijerink, P. Van Der Voort, *Angew. Chem., Int. Ed.* **2021**, *60*, 3727-3736.

[28] X. Li, Q. Gao, J. Wang, Y. Chen, Z.-H. Chen, H.-S. Xu, W. Tang, K. Leng, G.-H. Ning, J. Wu, Q.-H. Xu, S. Y. Quek, Y. Lu, K. P. Loh, *Nat. Commun.* **2018**, *9*, 2335.

[29] Y. Shi, S. Wang, W. Tao, J. Guo, S. Xie, Y. Ding, G. Xu, C. Chen, X. Sun, Z. Zhang, Z. He, P. Wei, B. Z. Tang, *Nat. Commun.* **2022**, *13*, 1882.

[30] S. Nandi, H. D. Singh, P. Shekhar, D. Chakraborty, R. Kushwaha, V. Ramanathan, *J. Mater. Chem. A* **2023**.

[31] a) J. Häcker, D. H. Nguyen, T. Rommel, Z. Zhao-Karger, N. Wagner, K. A. Friedrich, *ACS Energy Lett.* **2022**, *7*, 1-9; b) S. Wahl, S. M. El-Refaei, P. Amsalem, A. G. Buzanich, N. Koch, N. Pinna, *Catal. Sci. Technol.* **2020**, *10*, 517-528; c) M. El-Roz, H. Awala, F. Thibault-Starzyk, S. Mintova, *Sens. Actuators B Chem.* **2017**, *249*, 114-122.

[32] a) X.-X. Wang, B. Junker, C. Ewald, U. Weimar, X. Guo, N. Barsan, *J. Phys. Chem. Lett.* **2022**, *13*, 3631-3635; b) H. Issa Hamoud, L. Wolski, I. Pankin, M. A. Bañares, M. Daturi, M. El-Roz, *Top. Curr. Chem.* **2022**, *380*, 37; c) M. El-Roz, P. Bazin, T. Birsa Čelič, N. Zabukovec Logar, F. Thibault-Starzyk, *J. Phys. Chem. C.* **2015**, *119*, 22570-22576.

[33] G. Das, S. Nagaraja, V. Sridurai, D. B. Shinde, M. Addicoat, T. Prakasam, F. Gándara, F. Ravaux, S. K. Sharma, G. G. Nair, Z. Lai, R. Jagannathan, M. A. Olson, A. Trabolsi, *Chem. Mater* **2019**, *31*, 4148-4155.

[34] B. Aradi, B. Hourahine, T. Frauenheim, *J. Phys. Chem. A* **2007**, *111*, 5678-5684.

[35] J. Řezáč, *J. Chem. Theory Comput.* **2017**, *13*, 4804-4817.

[36] a) H. Singh, M. Devi, N. Jena, M. M. Iqbal, Y. Nailwal, A. De Sarkar, S. K. Pal, *ACS Appl. Mater. Interfaces* **2020**, *12*, 13248-13255; b) Y. Liang, M. Xia, Q. Yu, Y. Li, Z. Sui, Y. Yuan, X.-M. Hu, Q. Chen, N. Wang, *Adv. Compos. Hybrid Mater.* **2022**, *5*, 184-194; c) S. Mitra, S. Kandambeth, B. P. Biswal, A. Khayum M, C. K. Choudhury, M. Mehta, G. Kaur, S. Banerjee, A. Prabhune, S. Verma, S. Roy, U. K. Kharul, R. Banerjee, *JACS* **2016**, *138*, 2823-2828; d) Q.-W. Meng, S. Wu, M. Liu, Q. Guo, W. Xian, X. Zuo, S. Wang, H. Yin, S. Ma, Q. Sun, *Sci. Adv.* **2023**, *9*, eadh0207; e) L. Zhao, X. Ma, J. Xiong, Q. Zhou, W. Chen, Z. Yang, F. Jiang, S. Wang, X. Yang, H. Bai, *J. Environ. Chem. Eng.* **2023**, *11*, 110549; f) P.-F. Mu, L. Zhang, R. Bu, L.-F. Xiong, Y.-W. Liu, E.-Q. Gao, *ACS Appl. Mater. Interfaces* **2023**, *15*, 6902-6911.

[37] Y. Chen, J. Qiu, X.-G. Zhang, H. Wang, W. Yao, Z. Li, Q. Xia, G. Zhu, J. Wang, *Chem. Sci.* **2022**, *13*, 5964-5972.

[38] Y. Sekine, T. Ikeda-Fukazawa, *J. Chem. Phys.* **2009**, *130*.

[39] M. e. Frisch, G. Trucks, H. Schlegel, G. Scuseria, M. Robb, J. Cheeseman, G. Scalmani, V. Barone, G. Petersson, H. Nakatsuji, Gaussian, Inc., Wallingford CT, **2016**.

[40] J. Binns, M. R. Healy, S. Parsons, C. A. Morrison, *Acta Crystallographica Section B: Structural Science, Crystal Engineering and Materials* **2014**, *70*, 259-267.

[41] J. S. Binkley, J. A. Pople, W. J. Hehre, *JACS* **1980**, *102*, 939-947.

[42] A. McLean, G. Chandler, *Chem. Phys.* **1980**, *72*, 5639-5648.

[43] G. Zhang, C. B. Musgrave, *J. Phys. Chem. A* **2007**, *111*, 1554-1561.

[44] a) M. Xu, L. Hua, L. Gong, J. Lu, J. Wang, C. Zhao, *Sci. China Chem.* **2021**, *64*, 1770-1777; b) N. V. Nucci, J. M. Vanderkooi, *J. Phys. Chem. B* . **2005**, *109*, 18301-18309.

Entry for the Table of Contents

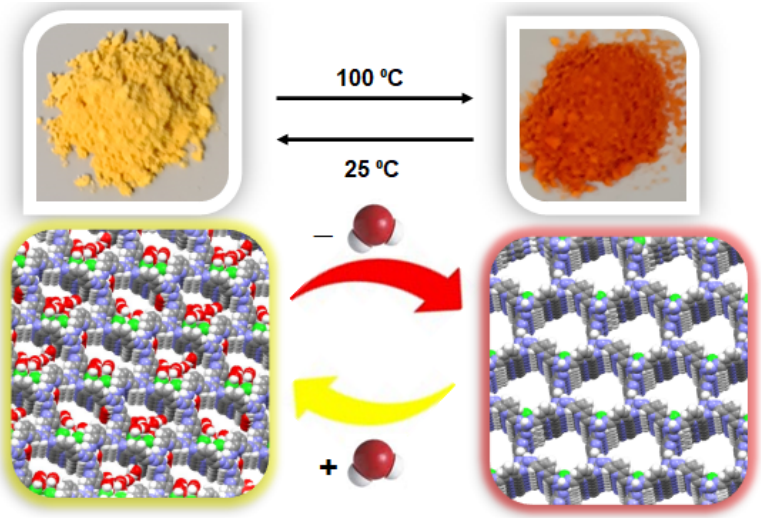

✓ Optical thermo-sensor
✓ Optical hygro-sensor
✓ Low temperature Luminescent
✓ Trace water detection in organic solvent

In this research, we have created a versatile cationic covalent organic framework, TG-DFP COF, using a simple microwave-assisted synthesis method. This material displays remarkable sensitivity to two crucial environmental factors: humidity and temperature. These parameters have a significant impact on its optical properties, and we have harnessed our COF to serve as a solid-state sensor for rapid and accurate measurement of temperature and humidity. The exceptional water sensitivity of our COF material has also led us to consider its potential as a candidate for detecting trace amounts of water in organic solvents.

Institute and/or researcher Twitter usernames:

https://twitter.com/gobindaaus

https://twitter.com/Fayrouz0111

https://twitter.com/TrabolsiAli